

# A Self-Tuning WEC Controller For Changing Sea States

Dominic D. Forbush, Giorgio Bacelli, Steven J. Spencer, Ryan G. Coe, David G. Wilson and Bryson Robertson

**Abstract**—A self-tuning proportional-integral control law prescribing motor torques was tested in experiment on a three degree-of-freedom wave energy converter. The control objective was to maximize electrical power. The control law relied upon an identified model of device intrinsic impedance to generate a frequency-domain estimate of the wave-induced excitation force and measurements of device velocities. The control law was tested in irregular sea-states that evolved over hours (a rapid, but realistic time-scale) and that changed instantly (an unrealistic scenario to evaluate controller response). For both cases, the controller converges to gains that closely approximate the post-calculated optimal gains for all degrees of freedom in a sufficiently short-time for realistic sea states. In addition, electrical power was found to be relatively insensitive to gain tuning over a broad range of gains, implying that an imperfectly tuned controller does not result in a large penalty to electrical power capture. Because the controller relies on an identified model of device intrinsic impedance, the sensitivity of power capture was evaluated with respect to uncertainty in the constituent terms of intrinsic impedance. Power capture is found to be relatively insensitive to uncertainty of 20% in constituent terms of the identified intrinsic impedance model. An extension of this control law that allows for adaptation to a changing device impedance model over time is proposed for long-term deployments, as well as an approach to explicitly handle constraints within this architecture.

**Index Terms**—wave energy, linear control, adaptive control, spectral analysis, feedback control

## I. INTRODUCTION

**H**ARVESTING energy from ocean waves presents a number of technical and practical challenges that must be overcome for this source of renewable energy to be economical. Intelligent control of a wave energy converter (WEC) can significantly enhance power capture and reduce overall cost of energy [1] [2]. Theoretically optimal control of a WEC requires advanced knowledge of the affecting wave [3]. While there is significant focus on accurate future-state wave prediction and prediction-based WEC control strategies [4],

Submitted 1 July 2021; revised 12 October, accepted 14 October, published 19 December 2022. This is an open access article distributed under the terms of the Creative Commons Attribution 4.0 license (CC BY <http://creativecommons.org/licenses/by/4.0/>). Unrestricted use (including commercial), distribution and reproduction is permitted provided that credit is given to the original author(s) of the work, including a URI or hyperlink to the work, this public license and a copyright notice. This article has been subject to single-blind peer review by a minimum of two reviewers.

This work received funding support from the US Department of Energy's Water Power Technologies Office.

D. Forbush, G. Bacelli, S. Spencer, R. Coe, and D. Wilson are with Sandia National Laboratories, Albuquerque, NM 87123, USA.

B. Robertson is with Oregon State University, Corvallis, OR 97331, USA.

Digital Object Identifier: <https://doi.org/10.36688/imej.5.327-338>

[5], [6], [7], this architecture adds complexity to implementation. The prediction is needed in real-time, which requires either a displaced or remote measurement of incoming waves and an accurate model of wave propagation, or a state-estimation procedure that can be computationally intensive. These approaches suffer on both a theoretical and practical basis. Theoretically, the utilization of a remote measurement and a state-estimation model are confounded in short-crested, multi-modal and depth varying conditions [8]. Under all of these conditions, the propagation and transformation of wave energy flux and associated parameters are poorly approximated via linear-wave models and require computationally intensive higher order methods. Practically, the vast majority of publicly available and robust datasets (both historical and current) are only reported in frequency domain spectral formats, and the necessary data from real-time prediction is either not available or company-specific intellectual property. Alternatively, approximations of theoretically optimal control that do not require prediction of future waves, but a frequency-domain estimate of the current sea-state have been pursued [9], [10]. Regardless of architecture, an ideal controller will optimize WEC performance over the changing sea-states to which the device will be subjected. These control strategies can capture > 90% of the energy of a complex conjugate controller [11]. This implies that a control law relying on a spectral estimate of the sea-state must update this estimate over time.

The present work investigates the performance of a proposed simple self-tuning control law in laboratory experiments that adjusts the motor torques of a three degree-of-freedom point absorber in changing sea-states to maximize electrical power capture. The control law uses a spectral estimation of the wave excitation forces that relies on an identified model of device intrinsic impedance. The performance of the control law is considered by comparing the gains resulting from the self-tuning approach to post-calculated optimal gains for a given sea-state. The accuracy of the spectral estimation and sensitivity of power capture to accurate model identification are also considered.

## II. METHOD

### A. WaveBot Device

The WaveBot is an axi-symmetric three degree-of-freedom (DOF) point absorber actuated in heave, pitch, and surge (Fig. 1). It has an outer radius of 0.88 m, a bottom radius of 0.35 m, and an overall height from the

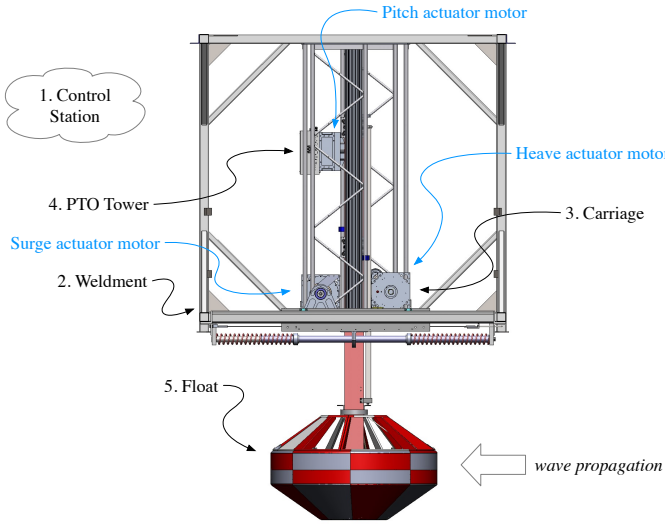


Fig. 1: Simplified diagram of the 3-DOF WaveBot device, axi-symmetric about the  $z$  (heave) axis [15].

flat bottom to the top of edge of the cylindrical surface (indicated with the red-white grid) of 0.73 m. In calm water, the free-surface of the device is 0.20 m below the top of the cylindrical surface. The rigid-body mass of the device is 893 kg in heave, 1420 kg in surge (which includes the surge carriage), and a rigid-body inertia in pitch of 84 kg-m<sup>2</sup>. It has identical independent permanent magnet brushless DC rotary motor/generators on each DOF connected to a common 300V DC bus. This allows for control force to be applied to the WEC via a belt transmission system (heave and surge) or a driveshaft and a float-contained gearhead (pitch). Velocities in each degree of freedom are measured from shaft-mounted motor encoders (heave and surge) or an inertial motion unit in the float (pitch).

The control system is connected via an EtherCAT network to a Simulink Real-time target computer, so that sensing and control is handled in a Simulink model. The device was tested in the Naval Surface Warfare Center Carderock Maneuvering and Sea-Keeping basin (MASK). Further details regarding device design and testing facility are given in [12], [13], [14].

### B. Control Approach

The theoretically optimal power-maximizing control law for an ideal WEC device uses a compensator that is the complex conjugate of the WEC intrinsic impedance, that is, the complex ratio of the device velocity to imposed force in the frequency domain. The non-causal nature of this controller implies that knowledge of the future input to the device is necessary for implementation on a real system [1]. However, complex conjugate control behavior can be approximated by a feedback controller over a finite range of frequencies [16]. Since the set of nearly all natural ocean waves show excitation over relatively narrow bandwidths [17], approximately 0.05 to 0.2 Hz, this approximation has practical application. Sea-states also evolve in time: this suggests that the approximated controller must be able to adapt to the given sea state, ideally with

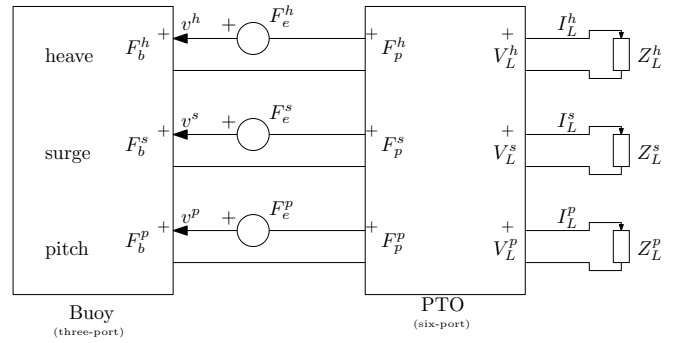


Fig. 2: Multi-Port representation on the WaveBot.

no additional sensing. This study proposes a control law that requires only an estimate of device intrinsic impedance and measurements of WEC velocities to maximize device electrical power over all DOFs in changing sea states.

The intrinsic impedance of a WEC follows from the general frequency-domain equations of motion [1]. By simply rearranging and collecting terms, the WEC intrinsic impedance can be defined,

$$Z_i(\omega) = i\omega(M + m(\omega)) + B_v + R(\omega) + \frac{S}{i\omega} \quad (1)$$

where  $M$  and  $m$  are the static and added inertia matrices for the device,  $B_v$  is the viscous damping matrix,  $R$  is the radiation damping matrix,  $S$  is the hydrostatic stiffness matrix, and  $\omega$  is the radian wave frequency. If the device geometry and basic mass properties are known, an estimate of  $Z_i$ , excluding viscous damping, for a WEC can be estimated from the outputs of a boundary-element method code. In this way, a model of device impedance suitable for initial controller development is available early in the design process. If a physical device exists, a model of the intrinsic impedance of the as-built device can be developed from experimental data via system identification techniques [18].

1) *Development of Device Model:* Beginning from a high-level model of power flow in the system, the WEC can be modeled as a two-block multi-port circuit (Fig. 2) [14]. The buoy block captures the hydrodynamic interactions between the device and the wave (forces/torques  $F_b$ , and velocities  $v$ ), and the power-take-off (PTO) describes the generators. In this model, the electrical power (to be maximized through controller design), is the sum of the powers (calculated from load voltages  $V_L$  and load currents  $I_L$ ) delivered to the electrical loads  $Z_L^h$ ,  $Z_L^s$ , and  $Z_L^p$ , where the superscripts  $h$ ,  $s$ , and  $p$  indicate the heave, surge and pitch DOFs, respectively (Fig. 2). Each DOF has an independent and identical PTO, thus the six-port model of the PTO is block diagonal and it can be represented as 3 two-port elements in matrix form as:

$$\begin{bmatrix} I_q^i \\ V_q^i \end{bmatrix} = \begin{bmatrix} 0 & (k_t^i n^i)^{-1} \\ k_e^i n^i & r(k_t^i n^i)^{-1} \end{bmatrix} \begin{bmatrix} v^i \\ F_p^i \end{bmatrix}, \quad (2)$$

where  $i$  is an index specifying the DOF ( $h$ ,  $s$ , or  $p$ ) and the parameters  $k_t^i$ ,  $k_e^i$ ,  $n^i$ , and  $r$  are the torque constant

(Nm/A), electrical constant (Vs/rad), transmission ratio (rad/m for heave and surge, rad/rad for pitch), and winding resistance (Ohm) respectively. Due to the identical PTOs,  $k_t = 6.17$ ,  $k_e = 4.12$ , and  $r = 0.50$  for all DOF, while  $n^{h,s} = 12.47$  but  $n^p = 3.00$  due to the inclusion of the gearhead on the pitch DOF.

A diagonal proportional-integral controller form was selected due to its broad familiarity,

$$C = \begin{bmatrix} K_p^h + \frac{K_i^h}{s} & 0 & 0 \\ 0 & K_p^s + \frac{K_i^s}{s} & 0 \\ 0 & 0 & K_p^p + \frac{K_i^p}{s} \end{bmatrix}. \quad (3)$$

where  $s$  (non-superscript) is the Laplace transform variable. Note that the absence of off-diagonal terms implies that the controller does not respond to coupling between the surge and pitch degrees of freedom. As shown in Fig. 3, the controller uses a measurement of velocity in heave, surge, and pitch to prescribe a force to the motor on each DOF. A model of the transfer function  $H$  relating wave height to excitation force is not needed for controller tuning.

It can be shown (see [14] for details), that the average electrical power absorbed by the WEC for zero-mean excitation and control force, is

$$P_{abs} = \frac{3}{4} \mathcal{R} \left( (NK_t)^{-1} C \Omega \right)^* \left( (K_e N + R(NK_t)^{-1} C) \Omega \right) \quad (4)$$

where  $\Omega = [v^h, v^s, v^p]^T$  is the frequency-domain velocity vector, and  $K_t$ ,  $K_e$ ,  $R$ , and  $N$  are  $3 \times 3$  diagonal matrices of parameters  $k_t^{h,s,p}$ ,  $k_e^{h,s,p}$ ,  $r^{h,s,p}$ , and  $n^{h,s,p}$  respectively. In (4),  $*$  implies the complex conjugate, and script  $\mathcal{R}$  implies the real part. By the sign convention of  $C$ ,  $P_{abs} < 0$  for power absorbed by the WEC (that is, power capture is optimized when  $P_{abs}$  is as negative as possible).

By simple manipulation of the block diagram (Fig. 3), it can further be shown that

$$\Omega = (Z_i - C)^{-1} F_e. \quad (5)$$

Thus, for a given excitation force spectra  $F_e$ , and device intrinsic impedance model  $Z_i$  (a  $3 \times 3$  model), the minimum absorbed power  $P_{abs}$  is attained for an optimal set of controller gains  $\eta_{opt} = \{K_p^h, K_i^h, K_p^s, K_i^s, K_p^p, K_i^p\}$ , the result of the optimization

$$\eta_{opt} = \arg \min_{\eta} P_{abs}(\eta, F_e). \quad (6)$$

Using (4) this problem is solved iteratively in MATLAB via *'fminsearch'*, a gradient-free Nelder-Mead simplex optimizer, recalling that, by sign convention, a minimum of  $P_{abs}$  maximizes captured power. With the exception of the first calculation (for which rough order-of-magnitude initial guesses were used), optimal gain estimates from the previous time step are used as the initial guess at the current time step.

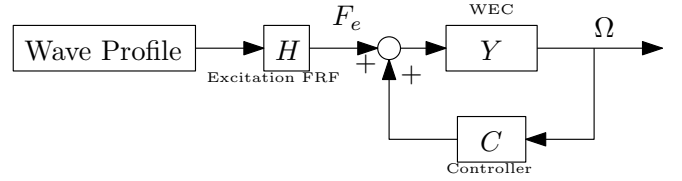


Fig. 3: Block diagram of the linear system model assumed for controller self-tuning. The inverse of the WEC intrinsic impedance  $Z_i$  is used as the plant model.

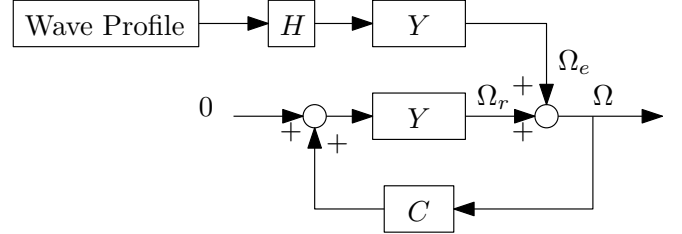


Fig. 4: Modified block diagram of the linear system model. In this case the effects of the waves are introduced as an output disturbance  $\Omega_e$ .

2) *Estimation of Excitation Force*: Equation 6 requires a frequency-domain estimate of the excitation force spectra and a model of device intrinsic impedance. To obtain the latter, the device was subjected to multi-sine excitation in all DOFs, with different phase realizations in each, such that motions in each DOF were uncorrelated. The system identification procedure of [12] was then employed to generate a non-parametric frequency-domain estimate of intrinsic device impedance  $Z_i$ , over the frequencies of interest (0.05 to 2 Hz). Considering the simplified linear model (Fig. 3), where  $Y$  is the inverse of the impedance model, measured WEC velocity spectra,  $V(\omega)$ , and controller force spectra,  $F_{control}(\omega)$ , can be used to estimate the excitation force spectra  $F_e$

$$F_e = Z_i V - F_{control} \quad (7)$$

for each DOF. Frequency domain estimates of  $V(\omega)$  and  $F_{control}(\omega)$  were obtained from real-time experimental time-domain measurements of WEC velocity,  $v(t)$ , and controller force,  $f_{control}(t)$ . First, time-domain measurements were down-sampled from 1 kHz to 4 Hz and then a Hamming window was applied to a buffer of 1024 points (i.e., 256 seconds). Subsequent windows overlap by 1020 points. A new window was sampled every 16 s, and the discrete Fourier transform was then applied to this window. Frequencies between 0.15 and 2 Hz are considered in (7), known *a priori* to bound the energy spectra of all selected wave cases (Table I), such that high-frequency noise or DC-offsets are not included in  $F_e(\omega)$  estimations. Spectral estimates were found to be largely insensitive to the extent of down-sampling, overlap, and window length, provided that windows were long enough to estimate the excited frequencies at sufficient resolution.

An alternative approach for the tuning of the controller can be obtained by considering the block diagram in Figure 4, which is equivalent to the one in

Figure 3. In this case, the velocity vector  $\Omega$  is the sum of two terms:  $\Omega_r$ , which is due to the radiation, and  $\Omega_e$  which is the contribution on the total velocity due to the waves, that is:

$$\Omega = \Omega_e + \Omega_r = \Omega_e + Z_i^{-1}C \Omega. \quad (8)$$

By solving for  $\Omega$ , the total velocity is now expressed as functions of the velocity contribution due to the waves, as

$$\Omega = (I - Z_i^{-1}C)^{-1}\Omega_e, \quad (9)$$

where  $\Omega_e$  can be calculated as

$$\Omega_e = V - Z_i^{-1}F_{control}. \quad (10)$$

Equations (9) and (10) are equivalent to (5) and (7) for a square system (i.e. the impedance matrix is square), that is for a system where there number of PTOs is equal to the number of degrees of freedom (i.e. the size of the velocity vector). By using (9) and (10) it is possible to apply the approach to more general non-square system where the number of PTOs is less than the number of DOFs, which is often the case for real systems. For these type of systems, in fact, it may not be possible to estimate the impedance matrix; however, the admittance matrix ( $Z^{-1}$ ) can always been obtained, for example, by means of system identification (i.e. forcing the PTO actuators and measure the velocity response).

### C. Changing Sea-States

The self-tuning control law was tested in variety of realistic and changing sea-states. In this work, we focus on two types of test cases: a) a 1/9th Froude-scaled time-series developed from Coastal Data Information Program (CDIP) ocean buoy 225 at the Wave Energy Test (WETS) site in Kanehoeh Bay, Hawaii, and b) an approximation of an ‘instantaneous’ change in sea-state created by abutting two wave time series from distinct irregular sea-states (Figure 5).

The WETS has been actively testing WEC concepts for almost 2 decades and provides ideal conditions for smaller scale WEC concepts due to the trade-winds dominated wind swell and the islands’ geography blocking the dominant, highly active northerly swell regimes. Thus, the test conditions utilized are widely representative of actual conditions for WEC control design. CDIP data records are unique from other ocean observation buoys in that they log a time-domain history of free-surface position. This particular period of buoy data was selected as it captures the sea-state evolution during an approaching storm, representing a rapid, though realistic, rate of change. The time history of free-surface position was scaled by the scaling factor (1/9), and the time (in seconds) was scaled by the square root ( $\sqrt{1/9}$ ), according to Froude scaling conventions. Irregular waves are defined by a JONSWAP spectra with  $\gamma = 3.3$  ([19]), and the shorthand wave ID codes are explained in Table I. The peak period  $T_p$  of the JONSWAP spectra were selected as they correspond approximately to the resonant frequency in heave and surge ( $\sim 3.5$  s) and the resonant frequency in pitch ( $\sim 1.6$  s).

TABLE I: Model-scale wave ID codes.

Wave ID	Type	$T_p$ (s)	$H_s$ (m)
2A	JONSWAP	1.58	0.127
10A	JONSWAP	3.5	0.254
CDIP	Data	Varies	Varies

To evaluate controller performance, each wave case was run a minimum of 2 times. During one of these runs, the WEC was removed from the water. Wave height sensors at the nominal device location were used to characterize the exciting wave field without the influence of device-initiated wave reflections or radiations. This measured wave state can be compared to that estimated via (7) to evaluate the performance of the spectral estimator.

### III. EFFECT OF MODEL UNCERTAINTY

Although the controller under consideration is fundamentally a feedback controller, the gain selection is informed by an open-loop model of device impedance. As a result, errors in the utilized model, introduced either during the system identification process, or as a result of changes to device dynamics over time, will lead to sub-optimal gain selection and diminish controller performance. To examine the sensitivity of the self-tuning approach to model uncertainty, errors are introduced to the ‘true’ impedance model

$$Z_{error} = Z_i + \Delta Z = Z_i + \Delta B + j(\omega \Delta M - \Delta K/\omega) \quad (11)$$

where errors introduced to the inertia ( $\Delta M$ ), spring stiffness ( $\Delta K$ ), and damping ( $\Delta B$ ) terms are  $3 \times 3$  matrices. The elements of this matrix are random numbers drawn from a normal distribution with standard deviations equal to percentages of quantities estimated from nominal models. For the diagonal elements,  $\Delta M$  is a percentage of the infinite frequency added inertia  $A_{inf}$ ,  $\Delta K$  is a percentage the hydrostatic stiffness coefficient  $S$ , and  $\Delta B$  is a percentage the maximum value of the damping coefficient for each degree of freedom  $R_{max}$ .

$$A_{inf} = \begin{bmatrix} 822 & 0 & 0 \\ 0 & 155 & 114 \\ 0 & 114 & 96 \end{bmatrix} \quad (12)$$

$$S = \begin{bmatrix} 23707 & 0 & 0 \\ 0 & 0 & 534 \\ 0 & 215 & 5500 \end{bmatrix} \quad (13)$$

$$R_{max} = \begin{bmatrix} 1628 & 0 & 0 \\ 0 & 1143 & 152 \\ 0 & 189 & 336 \end{bmatrix} \quad (14)$$

For this device, where no coupling exists between the heave and other degrees of freedom, none was introduced through the addition of error (i.e., by definition  $\Delta Z_{1,2} = \Delta Z_{2,1} = \Delta Z_{1,3} = \Delta Z_{3,1} = 0$ ). However, the surge pitch degrees of freedoms are coupled, and so the  $\Delta B_{2,3}$  and  $\Delta B_{3,2}$  is the maximum of the magnitude of the real part  $Z_i$  for each element, and  $\Delta K_{2,3}$ ,  $\Delta K_{3,2}$  are the same with the imaginary part. Fifty realizations of  $Z_{error}$  were simulated at three different percentage

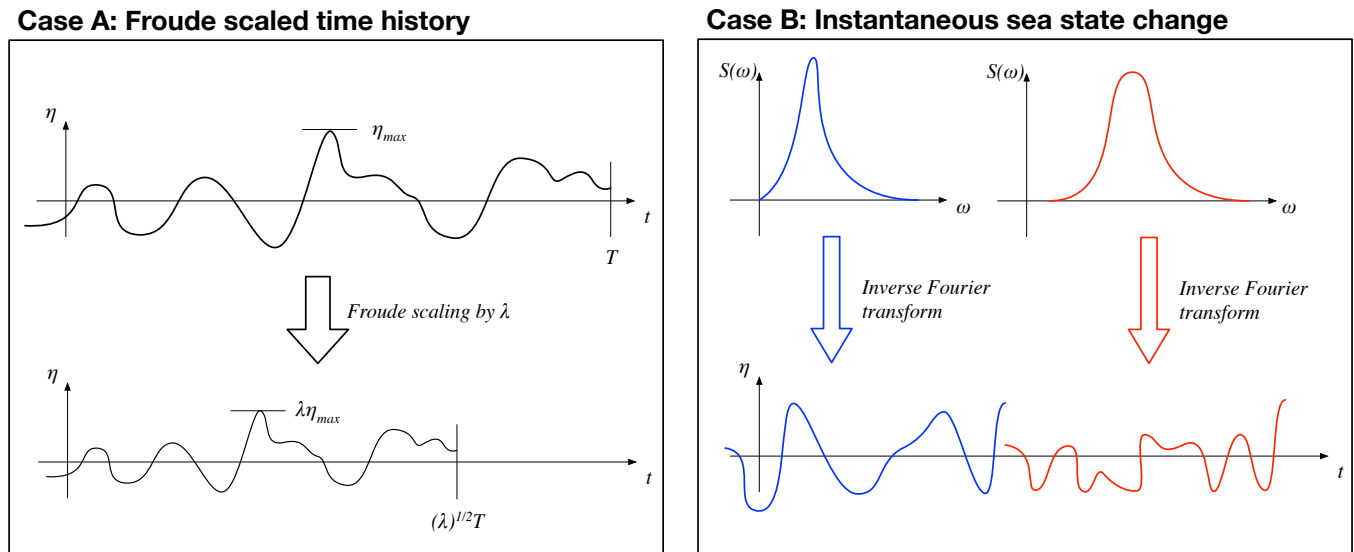


Fig. 5: Visualization of the procedure employed to create the scaled CDIP wave (a) and the approximation of an ‘instantaneous’ change in sea-state. Note that the discontinuity in the right plot time series exists only in the command to the wave maker: in reality, actuation limits at the wave maker and the physics of the basin ensure continuous dynamics that rapidly approximate the desired wave frequency content.

values intended to bound a mild, moderate and severe model error in two distinct sea states, 2A and 10A, and the gain combination resulting from the optimization and power capture were logged. Additionally, the effect on gain selection for independent errors in damping, spring stiffness, and inertia were examined qualitatively. Because the magnitude of  $\Delta Z$  over time can be employed as a device condition monitor, an understanding of gain behavior in the presence of particular estimation errors (e.g., underestimated damping) can imply specific device conditions and inform maintenance scheduling.

#### IV. RESULTS

A comparison between estimated excitation force spectra (7) and excitation force spectra calculated from measured wave height spectra at WEC location during the calibration study is calculated as

$$F_{e,actual}(\omega) = H(\omega)\eta(\omega) \quad (15)$$

where  $H$  is the identified  $1 \times 1$  transfer function between input wave height to output excitation force in heave. Of the 3 DOF, heave was selected for this calculation because it consistently showed the largest dynamic responses, resulting in a large signal-to-noise ratio across all sea-states. This estimate from measured wave height is compared to the heave DOF estimate used by the self-tuning controller from (7), which does not use a measurement of wave height or estimate of the excitation model.

To evaluate controller performance, an estimate of excitation force spectra (7) was used to calculate  $P_{abs}$  (4) over a dense grid of  $K_p$  and  $K_i$  gains for each

DOF. This allowed a  $P_{abs}(K_p, K_i)$  surface to be post-calculated for each sea state. The gains to which the self-tuning controller converged can be compared against the minima of these surfaces to consider the optimality of controller performance for that sea-state.

##### A. CDIP Buoy Sea-State

The spectrogram of wave spectra is shown with time series of controller gains in heave, surge, and pitch to show the adaptation over time (Fig. 6). Contrasting wave states at times 7000s (wave state 1, relatively calm water) and 24600s (wave state 2, a storm condition) are then examined in detail.

A comparison of the estimated spectra (7) to the actual spectra (15) is given in the first subplot of Fig. 6. Estimates for both wave states agree closely: the elevation in spectral energy at the decreased frequency for the second wave state is clearly seen in the estimate, although (7) tends to slightly over-predict excitation force at higher frequencies (0.8 to 1Hz), where the signal-to-noise ratios of the terms used in (7) are reduced. The reduced accuracy of the estimation in this range implies in turn that the WEC is less able to absorb power at these higher frequencies, but given the  $\sim 20$  dB reduction in magnitude at these frequencies, there is little power available.

Fig. 7 shows the location of the self-tuning controller gain as the black dot on the post-calculated power surface, and the optimal value of the post-calculated surface as the cross. Because heave is nearly independent from surge and pitch, the heave power surface is described as a function of  $K_p^h$  and  $K_i^h$ . However, due to the coupling of surge and pitch DOFs, their power

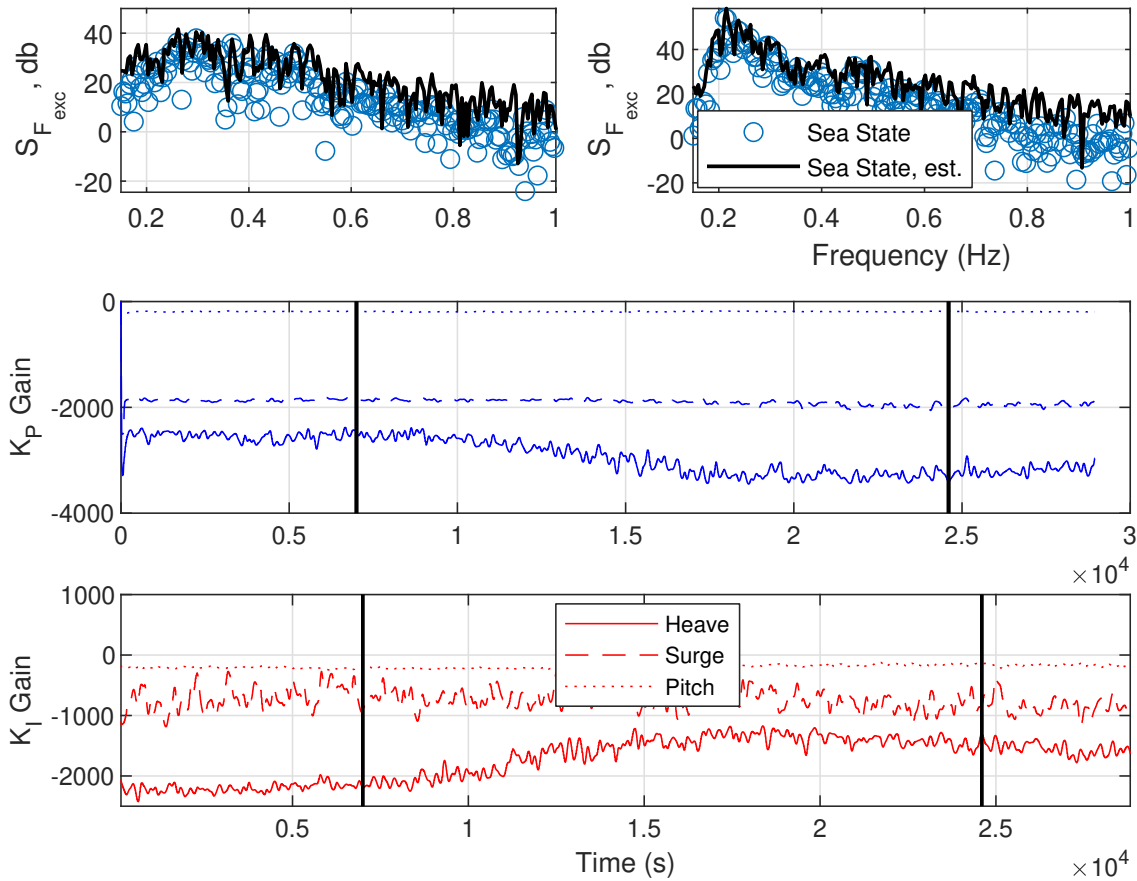


Fig. 6: Self-tuning controller gains for the CDIP225 wave state. Heave, surge, and pitch line styles are consistent across the lower two subplots.

surface is four-dimensional (two gains for each DOF). For visualization, a 2D slice was taken of this surface at the optimal surge gains (for the pitch subplot) and the optimal pitch gains (for the surge subplot) such that the self-tuning and optimal controller gains also appear on this slice.

Self-tuning gains are near the optimum of the power surface, which indicates a maximized WEC power production, for all degrees of freedom for both wave states. Note that the  $P_{abs}$  surface has small gradients near the optimum: this implies both that an optimizer may not reliably converge precisely to the minimum, and that system electrical power is not sensitive to gain selection within this region.

### B. Concatenated Sea-states

As an example of concatenated wave series, the spectrogram of wave spectra is shown for alternating sea-states 2A and 10A, switched every 5 minutes, with time series of controller gains in heave, surge, and pitch to show the adaptation over time (Fig. 8). Contrasting wave states at time 250 s and 1200 s, indicated by black vertical lines are then examined in detail.

Note that in this case, the peak wave period of state 2A is 1.58 s (0.63 Hz), which is nearly the WEC resonant frequency in heave ( $\sim 0.62$  Hz). As expected, the  $K_i^h$  is near zero during this wave state (at resonance, the optimal  $K_i$  gain is zero, ([9])). The explicitly known transition time of a concatenated wave series allows

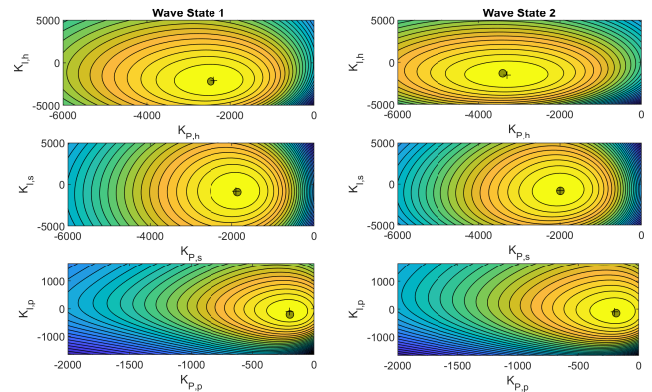


Fig. 7: The WEC power surface as a function of gain tuning for each degree of freedom and wave state for the CDIP 225 wave. Optimal absorbed power is the brightest yellow.

consideration of the gain adaptation time: the wave state command is changed at multiples of 300 s (i.e., at  $t = [300, 600, \dots]$ ), and the gain adjustment is shown to begin approximately 200 s after this. The delay is due to two factors. Firstly, inspection of the spectrogram indicates that the commanded wave transition takes approximately 60 s to manifest in the basin. Second and more significantly, the window length of 256 s will only fully reflect the next sea state after this length of time, and the interim gain will be calculated based upon an

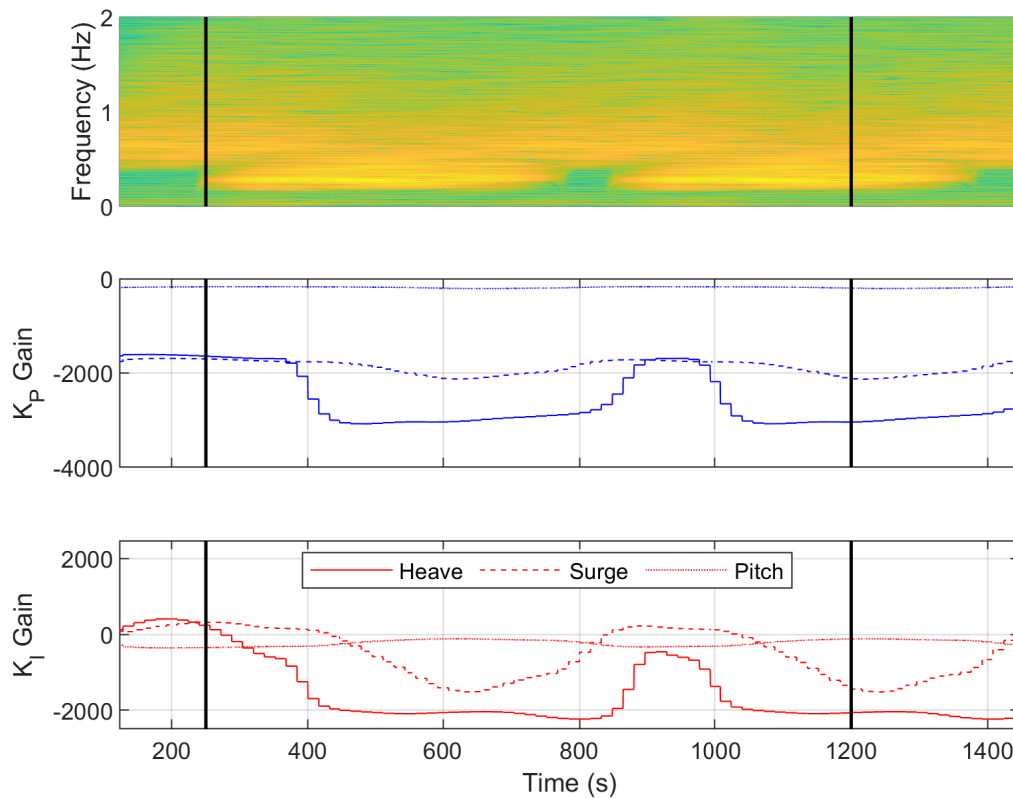


Fig. 8: Self-tuning controller gains for changing 2A-10A wave state. Heave, surge, and pitch line styles are consistent across subplots.

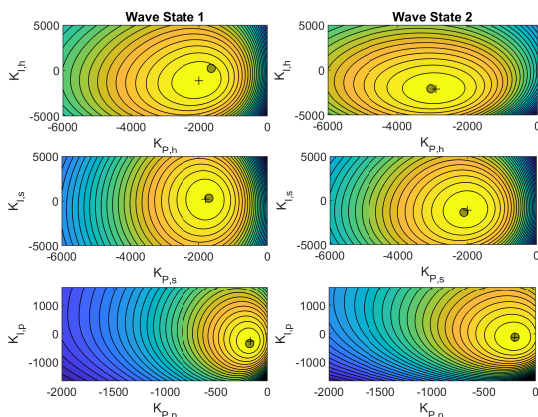


Fig. 9: The WEC power surface as a function of gain tuning for each degree of freedom and wave state for the 2A-10A concatenated wave. Optimum absorbed power is the brightest yellow. The post-calculated optimal gain combination for the sea state is shown as the +, while the combination of gains suggested by the autotuner at the investigated instant is shown by the transparent dot.

average of the two wave states. Accounting for these delay contributions, the gain adapts fairly quickly. The estimated excitation spectra (not shown) predict excited frequencies well, but again slightly over-estimate amplitudes of higher frequencies ( $f > 0.7$  Hz).

The power surfaces for this wave series (Fig. 9)

indicate that the self-tuning controller gains (dots) are again near the maximum of the post-calculated surface (crosses), which is again flat in the surrounding region, for each wave state and degree of freedom. The largest deviation from the minimum occurs for heave in the first wave state: however, power captured by the self-tuning gains are within 1% of the maximum post-calculated power. The minima locations change more significantly for heave than for surge and pitch, indicating the latter modes to be less sensitive to this change in sea state.

### C. Model Uncertainty

The effect on the generated impedance model with added errors is shown in Figure 10, where  $Z_i$  is shown with fifty realizations of  $Z_{error}$  with 20% standard deviation in all three parameters. The estimated resonant frequency is affected, particularly in the pitch DOF. In all DOFs, the magnitude of the impedance varies in excess of 20 db.

Inspecting the resulting gain tunings, for sea-state 10A the heave degree of freedom has a narrow range of  $K_{I,h}$  and a pronounced spread of  $K_{P,h}$  from approximately -2000 to -3400 (Figure 11). This suggests that the reactive  $K_{P,h}$  term is more sensitive to model uncertainty for this device in this degree of freedom for this sea state, while power (illustrated by the steepness of the contour) is itself more sensitive to  $K_i$  selection. Nonetheless, the worst-case realization in heave captured 96.2% of the electrical power obtained using the true  $Z_i$ , and 96.7% of total electrical power (Table

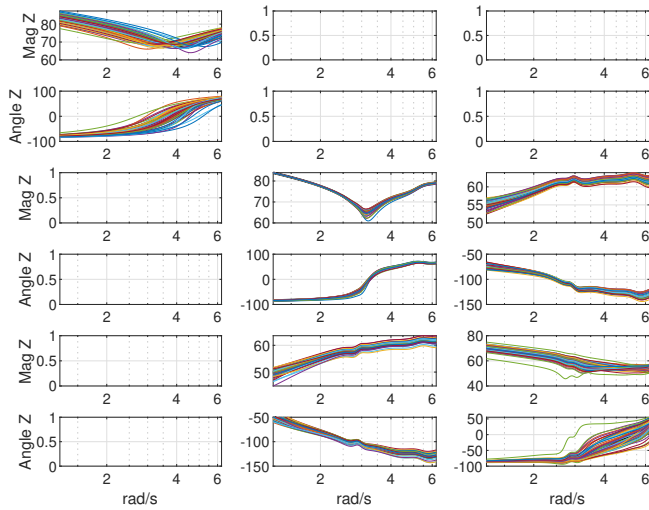


Fig. 10: Fifty realizations of impedance model  $Z_{error}$  with 20% uncertainties on inertia, spring, and damping terms

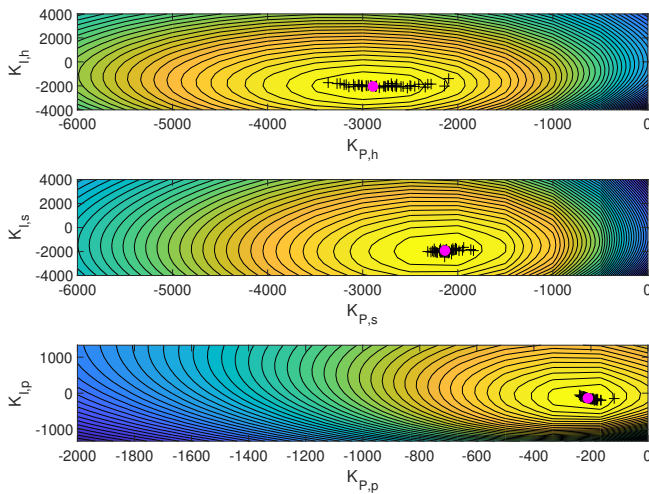


Fig. 11: The  $P_{abs}$  surface, shown with fifty realizations of impedance model  $Z_{error}$  with 20% uncertainties on inertia, spring, and damping terms for sea-state 10A.

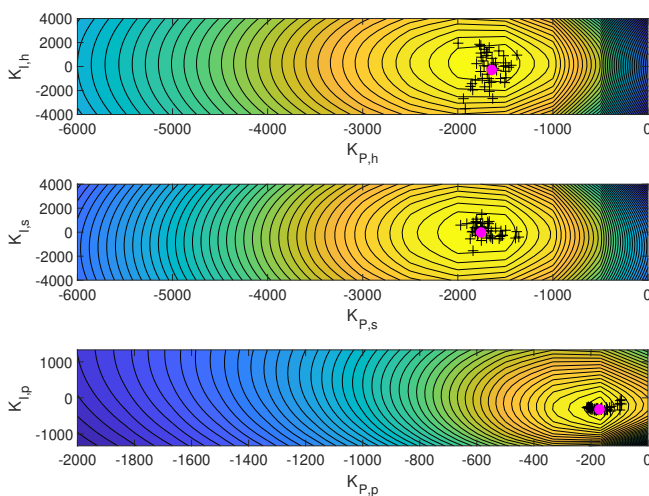


Fig. 12: The  $P_{abs}$  surface, fifty realizations of impedance model  $Z_{error}$  with 20% uncertainties on inertia, spring, and damping terms for sea-state 2A.

II). The median of power capture from all  $Z_{error}$  was greater than 99% in all DOF for this sea-state (Table III).

Lower sensitivity in  $K_P$  is demonstrated in the coupled surge/pitch degree of freedom, but it is still markedly more sensitive than  $K_I$ . Most of the power captured in this sea-state occurs in heave, suggesting the elevated sensitivity to modeling errors in this DOF.

Gain sensitivities are somewhat distinct in the shorter-period sea-state (2A, Figure 12). The pitch DOF sees more substantial excitation in this sea-state, and as a result, modeling errors in the surge/pitch degree of freedom affect power capture more severely (Tables II and III). Heave and surge  $K_I$  gains show an elevated sensitivity to modeling error. This is somewhat intuitive: In this sea-state, both are further from resonance, and the reactive term plays a more substantial role in controller response. In this sea state, power capture was more affected, with worst-case total power capture 88.6% of that of  $Z_i$ , and a median power total power of capture 98.6%. A decrease in modeling uncertainty increases power capture monotonically in all cases (Tables II and III).

Considering the separate effects of inertia, damping, and stiffness uncertainties separately, we note that the characteristics of the optimal gains for each error constituent varies considerably with sea-state. The objective of this controller is, fundamentally, to approximate the complex conjugate of device impedance  $Z_i$ . Uncertainties in damping will affect the real part of the impedance, and it is therefore expected that  $\Delta B$  will more substantially impact  $K_P$ , while  $\Delta M$  and  $\Delta K$ , which influence the imaginary part of the impedance, will have more impact on  $K_I$ , but the effect on power will depend on the sea-state, specifically how far excited frequencies are from natural device resonance which will dictate the relative importance of the reactive control term.

Additionally, the value of uncertainty used was a percentage of a fixed value for each sea-state. In the case of damping, the radiation damping coefficient is in fact a function of frequency. Specifically, the damping uncertainty near resonance for a particular DOF represents a smaller portion of the modeled damping, since at resonance this quantity is maximized, than it will at another sea-state. Thus, sea-state 10A, which is near resonance for heave, shows comparatively low sensitivity in heave to damping uncertainty (Figure 17) than in sea-state 2A (Figure 18). Similarly, sea-state 2A shows higher sensitivity to  $\Delta K$  in surge and pitch DOFs than 10A (Figures 15 and 16). In heave,  $K_p$  shows a significant range for sea-state 10A, while  $K_I$  shows a similar significant range in sea-state 2A, repeating the trend observed for 20% uncertainty in all constituents.

Across both examined sea-states, power capture appears the most sensitive to a perturbation of the stiffness term  $\Delta K$ , which showed worst-case power capture of 90.2% in sea-state 2A, and 96.4% in sea-state 10A (Table II). This is substantially higher than the effect of the next most-sensitive constituent perturbation. In sea-state 2A, the next lowest total power capture is 99.0% for a 20% uncertainty in  $\Delta M$ , and in sea-state

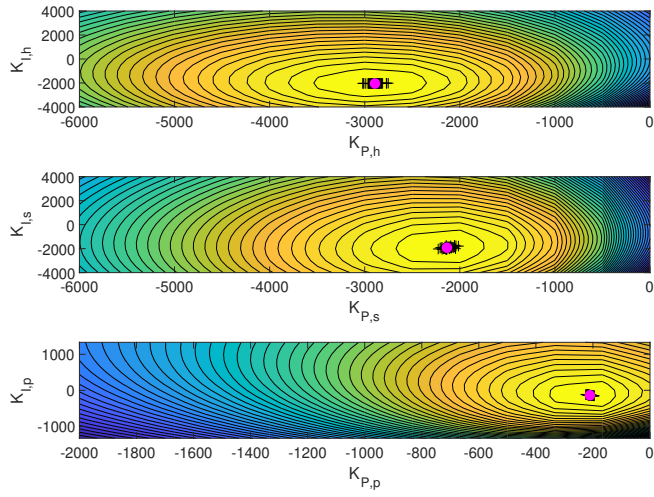


Fig. 13: Gain tunings for 20% uncertainty in the inertial term for sea-state 10A.

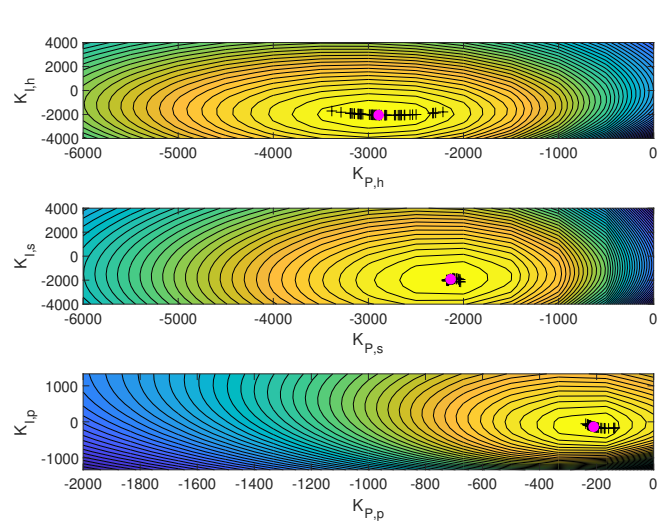


Fig. 15: Gain tunings for 20% uncertainty in the stiffness term for sea-state 10A.

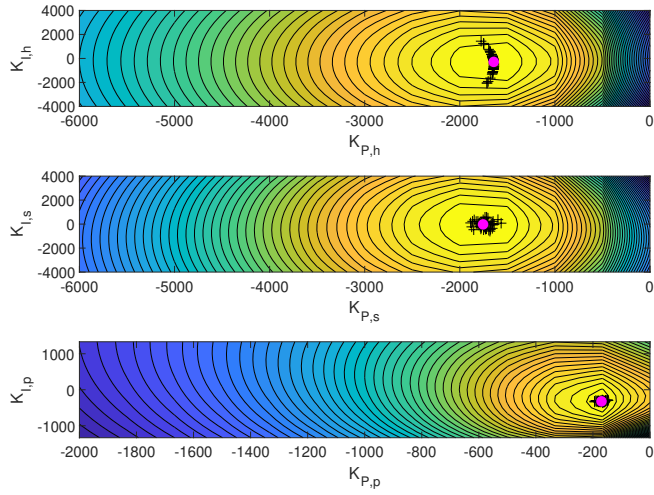


Fig. 14: Gain tunings for 20% uncertainty in the inertial term for sea-state 2A.

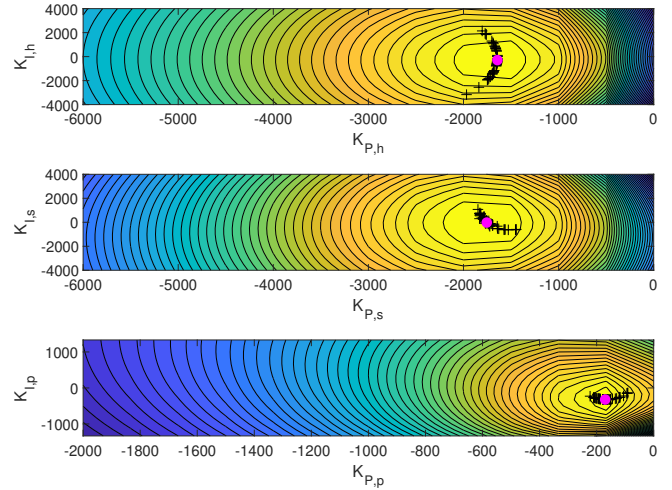


Fig. 16: Gain tunings for 20% uncertainty in the stiffness term for sea-state 2A.

10A, the next lowest total power capture is 99.9%.

V. DISCUSSION

Wave conditions, and their associated excitation on WEC devices, change via both known daily and seasonal cycles, but also via discrete storm events. Daily changes, due to adiabatic wind conditions in near-shore environments, and seasonal cycles, due to global distribution of solar insolation, are well known and can be reasonably characterized through long-term

TABLE II: Worst-case electrical power capture for introduced modeling error for sea-state 2A and 10A in heave (H), coupled surge and pitch (SP), and the total (T)

	2A			10A		
	H	SP	T	H	SP	T
5%, All	98.5	99.2	99.4	99.7	99.7	99.8
10%, All	94.7	96.2	97.1	99.0	98.5	99.2
20%, All	85.3	85.1	88.6	96.2	92.9	96.7
20% $\Delta_M$	97.1	99.0	99.0	99.8	99.7	99.9
20% $\Delta_D$	98.4	99.5	99.4	99.9	99.8	99.9
20% $\Delta_K$	91.8	87.4	90.2	95.7	93.9	96.4

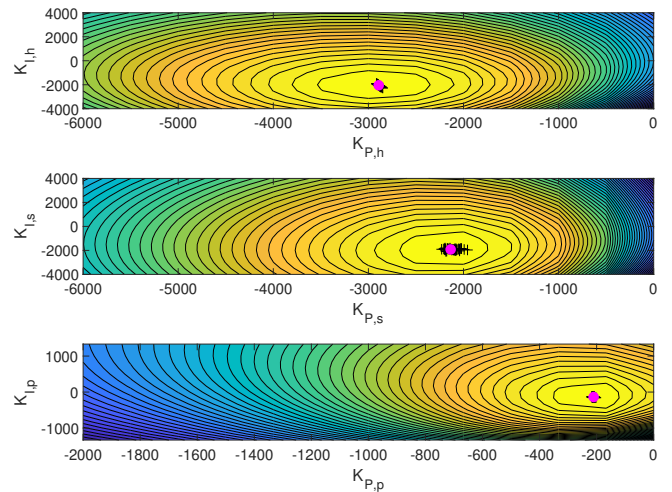


Fig. 17: Gain tunings for 20% uncertainty in the damping term for sea-state 10A.

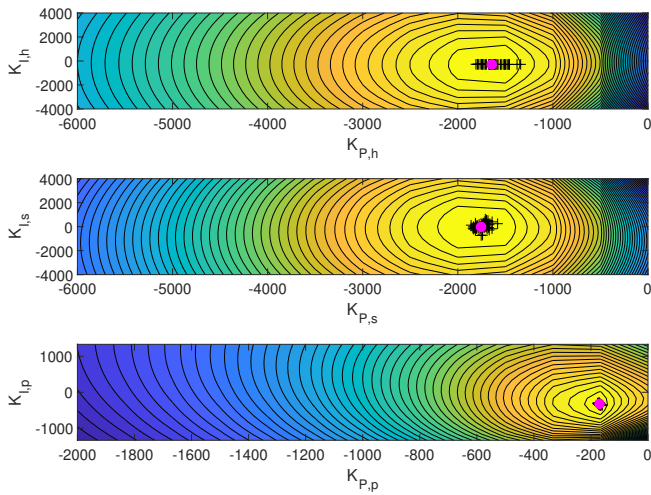


Fig. 18: Gain tunings for 20% uncertainty in the damping term for sea-state 2A.

TABLE III: Median electrical power capture for introduced modeling error for sea-state 2A and 10A in heave (H), coupled surge and pitch (SP), and the total (T)

	2A			10A		
	H	SP	T	H	SP	T
5%, All	99.9	99.9	99.9	99.9	99.9	99.9
10%, All	99.7	99.7	99.6	99.9	99.9	99.9
20%, All	99.0	98.9	98.6	99.8	99.6	99.5
20% $\Delta_M$	99.7	99.8	99.7	100	100	100
20% $\Delta_D$	99.9	99.9	99.9	99.9	99.9	99.9
20% $\Delta_K$	99.1	99.5	99.3	99.7	99.8	99.6

measurements and numerical hindcasts. Shorter term storm events can rapidly change sea state conditions in a matter of hours. These storm events both provide unique opportunities for power generation, but also require unique control algorithms to properly adjust operation.

A six-parameter self-tuning controller was implemented successfully in real-time with 1 KHz sampling on a real-time target machine with two 1.4 GHz processors with a mean execution time of  $8.53e-5$  s: an execution time  $> 10x$  faster than necessary to execute this sampling rate in real time on the small-scale device, which requires faster sampling than an equivalent full-scale device. Gains converged quickly once the buffer from which the spectral estimate was calculated well-approximated the current wave state: particularly for concatenated wave states, the 256 s buffer window appears to significantly delay gain tuning. While it is likely possible to reduce this window time, it is not likely to be necessary in a realistic sea, where conditions change more slowly. The present spectral estimate is robust and accurate, and convergence to optimal gains is on the order of minutes. While this is an infeasible delay for sea-states changing on the order of minutes, as in the concatenated wave tests, this is more than adequate for sea states changing over realistic time scales (hours to days), as evidenced particularly by the CDIP225 sea-state investigated in Section 4.

Negative values of  $K_i$  provide optimum power cap-

ture for sea-states where excitation frequencies are lower than WEC resonance by acting as a negative spring, counter-acting hydrostatic restoring stiffness and reducing system resonant frequency. Provided these negative gains do not overcome the hydrostatic stiffness of the device, the system can remain closed-loop stable. This stability bound was not explicitly enforced in the described optimization, and while the tuning procedure never approached instability, incorporating limits on gain values would increase the robustness of the self-tuning controller.

Converged self-tuning gains consistently find the optimal gains for each degree of freedom and wave state. Thus, the performance of the self-tuning controller is commensurate with the PI controllers investigated in [20], which attain nearly theoretical limits on performance over a finite bandwidth, resulting in  $\sim 90\%$  power capture compared to optimal complex conjugate control in realistic sea states. The flatness of the electrical power surface near the optimal gain selection in all examined wave cases suggests that this may be a robust feature of this particular device that is not likely to vary significantly with wave state, and the electrical power production is not particularly sensitive to gain selection. This may not be necessarily true for other WEC architectures and would need investigation prior to broad application.

While the PI controller relies on feedback, the *fmin-search* gain-tuning procedures are open-loop structure, using the model of device intrinsic impedance. Any inaccuracy in this model, or a change in the system over a long deployment could reduce the efficacy of this method. The intrinsic impedance estimation procedure can be periodically repeated to provide a revised estimate, however, highly accurate identified impedance models were not found to be necessary: a standard deviation of 10% in the estimation of damping, stiffness, and inertia components of impedance yielded nearly optimal gain parameters even in the presence of the introduced errors. It is only for standard deviations of 20% where more substantial reductions in captured power were observed: in the worst observed case, total electrical power capture was reduced by 11.4%. Even at this high uncertainty level, median power capture over all of the  $Z_{error}$  realizations reduced only 1.4%. This suggests that the proposed optimization is fairly insensitive to 20% uncertainty in the impedance model parameters. Larger uncertainties ( $\sim 50\%$ ) were introduced and in some cases caused an unstable selection of gains and a severe reduction in power capture. However, in all such cases, the open-loop impedance model estimated was itself unstable and thus easily deduced as erroneous.

In isolation, errors introduced in the hydrostatic stiffness parameter were found to be the most impactful on device power capture for this device. This suggests that efforts to estimate  $Z_i$  initially or adapt this estimate over a device deployment should attempt to characterize hydrostatic stiffness precisely, perhaps influencing test plans or sensor selection.

It is likely that the effect of modeling uncertainty will be more severe for monochromatic regular wave

excitation, in which an imperfect estimation of resonant frequencies will result in a gain tuning targeting a frequency with zero excitation (as opposed to the merely reduced excitation of an irregular wave field). In nature, regular wave fields do not exist, and conditions approaching regular wave fields are exceptionally uncommon, and thus this elevated sensitivity is of little practical concern.

With regard to software implementation, in order to run in real-time, the optimization must converge before the spectra are updated. This somewhat limits the allowable gain adjustment time. Further, if the optimization problem is not convex, convergence over any reasonable interval may not be ensured in real-time. In this instance, a look-up table correlating pre-calculated gains to the estimated sea-state could instead be employed. While selected gains cannot be proven to be globally optimal, they can be selected to deliver good performance and be attainable on WEC hardware.

Because this control law relies on the identification of a linear impedance model (or a family thereof) to estimate device behavior, it would be useful for other WEC devices for which these sorts of models are suitable. Similarly, the controller relies on this model to estimate the excitation force spectra resulting from the wave field: so long as this wave field is not exciting device behavior not predictable via the identified models (i.e., large or breaking waves) it will be useful in a more general multi-directional sea-state as well. The key step in the extension of this approach to other WECs and realistic seas is the robust identification of a suitable set of impedance models.

Finally, this control law is fundamentally single-objective and does not explicitly handle constraints. For longer deployments, it is necessary to also limit the structural loads experienced by the device. The magnitude of the loads experienced by the device can be related to the magnitude of the excitation spectra through identifiable transfer functions. This self-tuning control law can be generalized to any convex cost function. For this case, incorporating load-related terms in 6 would broaden control objectives, although the relative weighting between load-mitigating and power maximizing objectives would likely be determined on a case-by-case basis. With regard to constraints, it has been shown previously [21] that a "predictionless" model-predictive controller can be tuned to approximate PI control performance while also explicitly handling constraints. While it may be too computationally intensive to be reasonably implemented in real-time, this may be similarly handled via a look-up table, and suggests an additional step to the proposed control law that would use the identified PI control gains to subsequently derive a model-predictive controller that handles relevant constraints.

## VI. CONCLUSION

A adaptive linear feedback controller, that does not rely upon external measurements or future-state predictions of the sea-state, intended to maximize power

capture in evolving sea-states was tested in experiment. The controller was shown to perform well in both sea-states that evolved over realistic time-scales and those that change unrealistically rapidly. The adaptation time was significantly faster than what would be reasonably necessary in naturally occurring seas. The controller relies upon an identified linear model of the WEC intrinsic impedance and measurements of velocity and PTO force in each DOF to estimate excitation forces on the device and select optimal controller parameters. However, power capture was shown, in simulation, to be relatively insensitive to even substantial variations in this identified model. This suggests that the proposed controller is relatively tolerant to modeling error, and thus is likely to perform well even on long deployments, when wear, damage, or bio-fouling are expected to somewhat alter the intrinsic impedance of a deployed device. At present, optimal control parameters are considered to be those that maximize power capture. However, expanding the cost function to include load-related terms would allow this controller to potentially mitigate loads and achieve multiple objectives. This is an area suggested for future study.

## ACKNOWLEDGMENTS

DDF, GB, SJS, RGC, and DWG would like to acknowledge funding support from the US Department of Energy's Water Power Technologies Office. Sandia National Laboratories is a multi-mission laboratory managed and operated by National Technology and Engineering Solutions of Sandia, LLC., a wholly owned subsidiary of Honeywell International, Inc., for the U.S. Department of Energy's National Nuclear Security Administration under contract DE-NA0003525. This paper describes objective technical results and analysis. Any subjective views or opinions that might be expressed in the paper do not necessarily represent the views of the U.S. Department of Energy or the United States Government.

## REFERENCES

- [1] J. Falnes, *Ocean Waves and Oscillating Systems*. Cambridge; New York: Cambridge University Press, 2002.
- [2] J. Hals, J. Falnes, and T. Moan, "A comparison of selected strategies for adaptive control of wave energy converters," *Journal of Offshore Mechanics and Arctic Engineering*, vol. 133, no. 3, p. 031101, March 2011. [Online]. Available: <http://offshoremechanics.asmedigitalcollection.asme.org/article.aspx?articleid=1456895>
- [3] J. Falnes, "A review of wave-energy extraction," *Marine Structures*, vol. 20, no. 4, pp. 185–201, Oct. 2007. [Online]. Available: <http://www.sciencedirect.com/science/article/pii/S0951833907000482>
- [4] O. Abdelkhalik, R. Robinett, G. Bacelli, R. Coe, D. Bull, D. Wilson, and U. Korde, "Control optimization of wave energy converters using a shape-based approach," in *ASME Power & Energy*, San Diego, CA, 2015.
- [5] A. Babarit, G. Duclos, and A. Cl  ment, "Comparison of latching control strategies for a heaving wave energy device in random sea," *Applied Ocean Research*, vol. 26, no. 5, pp. 227–238, Jul. 2004. [Online]. Available: <http://www.sciencedirect.com/science/article/pii/S0141118705000209>
- [6] F. Fusco, J.-C. Gilloteaux, and J. Ringwood, "A study on prediction requirements in time-domain control of wave energy converters," in *Proceedings of the 8<sup>th</sup> IFAC Conference on Control Applications in Marine Systems*. Universitat Rostock, Germany: International Federation of Automatic Control, 2010.

- [7] R. G. Coe, G. Bacelli, V. Nevarez, H. Cho, and F. Wilches-Bernal, "A comparative study on wave prediction for WECs," Sandia National Laboratories, Tech. Rep. SAND2018-10945, 2018. [Online]. Available: <https://www.osti.gov/biblio/1476166-comparative-study-wave-prediction-wecs>
- [8] O. Kimmoun, H. Branger, and C. Kharif, "On short-crested waves: experimental and analytical investigations," *European Journal of Mechanical - B/Fluids*, vol. 18, no. 5, pp. 889–930, Sep. 1999.
- [9] H.-N. Nguyen and P. Tona, "Continuously adaptive PI control of wave energy converters under irregular sea-state conditions," in *Proceedings of the 12th European Wave and Tidal Energy Conference (EWTEC2017)*, Cork, Ireland, Aug 2017. [Online]. Available: <https://hal.inria.fr/hal-01628466/>
- [10] G. Bacelli and R. G. Coe, "Comments on control of wave energy converters," *IEEE Transaction on Control System Technologies*, pp. 1–4, February 2020. [Online]. Available: <https://ieeexplore.ieee.org/document/9005201>
- [11] R. G. Coe, G. Bacelli, and D. Forbush, "A practical approach to wave energy modeling and control."
- [12] G. Bacelli, R. G. Coe, D. Patterson, and D. Wilson, "System identification of a heaving point absorber: Design of experiment and device modeling," *Energies*, vol. 10, no. 10, p. 472, 2017. [Online]. Available: <http://www.mdpi.com/1996-1073/10/4/472>
- [13] R. G. Coe, G. Bacelli, S. J. Spencer, and H. Cho, "Initial results from wave tank test of closed-loop WEC control," Sandia National Laboratories, Albuquerque, NM, Tech. Rep. SAND2018-12858, 2018. [Online]. Available: <https://www.osti.gov/biblio/1531328-initial-results-from-wave-tank-test-closed-loop-wec-control>
- [14] R. G. Coe, G. Bacelli, S. J. Spencer, D. Forbush, and K. Dullea, "Advanced WEC dynamics and controls MASK3 test," Sandia National Laboratories, Albuquerque, New Mexico, Tech. Rep. SAND2019-15428, 12 2019. [Online]. Available: <https://www.osti.gov/biblio/1592850-advanced-wec-dynamics-controls-mask3-test>
- [15] G. Bacelli, S. J. Spencer, D. C. Patterson, and R. G. Coe, "Wave tank and bench-top control testing of a wave energy converter," *Applied Ocean Research*, vol. 86, pp. 351 – 366, 2019. [Online]. Available: <http://www.sciencedirect.com/science/article/pii/S0141118717307484>
- [16] V. Nevarez, G. Bacelli, R. G. Coe, and D. G. Wilson, "Feedback resonating control for a wave energy converter," in *Proceedings of SPEEDAM2018*, 2018. [Online]. Available: <https://ieeexplore.ieee.org/document/8445379>
- [17] W. H. Munk, "Origin and generation of waves," in *Proceedings of First Conference on Coastal Engineering*, Long Beach, CA, 1950.
- [18] L. Ljung, *System identification - Theory for the User*. Prentice-Hall, 1999.
- [19] K. Hasselmann, T. Barnett, E. Bouws, H. Carlson, D. Cartwright, K. Enke, J. Ewing, H. Gienapp, D. Hasselmann, P. Kruseman *et al.*, "Measurements of wind-wave growth and swell decay during the joint north sea wave project (JONSWAP)," *Ergänzungsheft 8-12*, 1973.
- [20] H. Cho, G. Bacelli, V. Nevarez, F. Wilches-Bernal, and R. Coe, "Evaluation of predictionless control for wave energy converters," in *EWTEC2019*, 2019. [Online]. Available: [https://www.researchgate.net/publication/338374910\\_Evaluation\\_of\\_predictionless\\_control\\_for\\_wave\\_energy\\_converters](https://www.researchgate.net/publication/338374910_Evaluation_of_predictionless_control_for_wave_energy_converters)
- [21] H. Cho, G. Bacelli, and R. G. Coe, "Model predictive control tuning by inverse matching for a wave energy converter," *Energies*, vol. 12, no. 21, p. 4158, Oct 2019. [Online]. Available: <http://dx.doi.org/10.3390/en12214158>